

Analyst

Accepted Manuscript



This is an *Accepted Manuscript*, which has been through the Royal Society of Chemistry peer review process and has been accepted for publication.

Accepted Manuscripts are published online shortly after acceptance, before technical editing, formatting and proof reading. Using this free service, authors can make their results available to the community, in citable form, before we publish the edited article. We will replace this *Accepted Manuscript* with the edited and formatted *Advance Article* as soon as it is available.

You can find more information about *Accepted Manuscripts* in the [Information for Authors](#).

Please note that technical editing may introduce minor changes to the text and/or graphics, which may alter content. The journal's standard [Terms & Conditions](#) and the [Ethical guidelines](#) still apply. In no event shall the Royal Society of Chemistry be held responsible for any errors or omissions in this *Accepted Manuscript* or any consequences arising from the use of any information it contains.



Journal Name

ARTICLE

Carbon quantum dots directly generated from electrochemical oxidation of graphite electrode in alkaline alcohols and the applications for specific ferric ion detection and cell imaging

Received 00th January 20xx,
Accepted 00th January 20xx

DOI: 10.1039/x0xx00000x

www.rsc.org/

Mengli Liu^{1,a}, Yuanhong Xu^{1,a}, Fushuang Niu^a, J. Justin Gooding^{b*}, Jingquan Liu^{a*}

Carbon quantum dots (CQDs) are attracting tremendous interest owing to their low toxicity, water dispersibility, biocompatibility, optical properties and wide applicability. Herein, CQDs with an average diameter of (4.0 ± 0.2) nm and high crystallinity were produced simply from the electrochemical oxidation of a graphite electrode in alkaline alcohols. The as-formed CQDs dispersion was colourless but it gradually changed to bright yellow when stored at room temperature. Based on UV-Vis absorption and fluorescence spectroscopy, X-ray photoelectron spectroscopy (XPS), Fourier transform infrared spectroscopy (FTIR) and high-resolution transmission electron microscopy (HRTEM), this colour change appeared to be due to oxygenation of surface species over time. Furthermore, the CQDs were used in specific and sensitive detection of ferric ion (Fe^{3+}) with broad linear ranges of 10 - 200 μM with a low limit of detection of 1.8 μM ($\text{S/N} = 3$). The application of CQDs for Fe^{3+} detection in tap water was demonstrated and the possible mechanism was also discussed. Finally, based on their good characteristics of low cytotoxicity and excellent biocompatibility, the CQDs were successfully applied to cell imaging.

1. Introduction

Carbon quantum dots (CQDs), are a reasonably new kind of fluorescent material with a diameter of less than 10 nm.¹ They have attracted considerable interest owing to their good biocompatibility, good cell permeability, low cytotoxicity, excellent dispersibility in water, flexibility in surface modification, chemical inertness and good optical performance.²⁻⁴ Thus, CQDs are considered as the next generation of green nanomaterials contributing to numerous promising potential applications including photoelectrocatalysis,⁵⁻⁸ targeted drug delivery,^{9, 10} photovoltaic devices,¹¹⁻¹³ sensing and bio-imaging.¹⁴⁻¹⁷ A range of approaches for synthesizing CQDs, since their first report in 2004,¹⁸ have been explored including electrochemical oxidation,^{2, 19, 20} chemical ablation,²¹⁻²³ microwave synthesis,^{24, 25} solution chemistry,²⁶ laser ablation,^{18, 27} arc discharge method,¹⁸ organic carbonization.^{1, 28-30} Many of these methods require relatively complicated procedures and stringent conditions. Recently, electrochemical methods have begun to

be intensely explored for the preparation of CQDs owing to advantages such as low cost, easy post-treatments, simple operation, high yield and good reproducibility.^{20, 31}

Different electrode materials can be used in the electrochemical generation of CQDs, such as graphite rod, carbon nanotube, carbon paste, carbon fiber and Pt sheets with the carbon source in electrolyte solution.^{5, 20, 32-34} Common electrolytes include ionic liquid (IL), acetonitrile containing 0.1 M tetrabutylammonium perchlorate and NaH_2PO_4 . The electrode materials and electrolytes are important as they can render the CQDs with different properties related to surface states, cytotoxicity and photoluminescence (PL) performance.^{2, 24, 35} Despite these achievements, there are still ongoing demands for developing more facile and efficient electrochemical methods for CQDs generation.

Inspired by the previous work, a graphite electrode, a platinum foil electrode and a Ag/AgCl electrode were used as working, counter, and reference electrodes, respectively, and the alkaline alcohols (e.g. NaOH/EtOH) were used as electrolyte to give a relatively economical and environment-friendly electrochemical system for the generation of CQDs. The colour of the CQDs was observed to change from colourless to bright yellow when exposed to air at room temperature. UV-Vis absorption spectra, fluorescence spectrophotometer, X-ray photoelectron spectroscopy and Fourier transform infrared spectroscopy suggested this colour change was due to oxidation of the CQDs. In addition, the obtained CQDs were employed for the specific and sensitive

^aCollege of Materials Science and Engineering; Laboratory of Fiber Materials and Modern Textile, the Growing Base for State Key Laboratory; Collaborative Innovation Center for Marine Biomass Fibers, Materials and Textiles of Shandong Province; Qingdao University, Qingdao 266071, China

E-Mail: jliu@qdu.edu.cn (J. Liu); Fax: +86 532 83780128; Tel: +86 532 83780128

^bSchool of Chemistry, Australian Centre for NanoMedicine and ARC Centre of Excellence in Convergent Bio-Nano Science and Technology, The University of New South Wales, Sydney, NSW 2052, Australia

E-Mail: justin.gooding@unsw.edu.au (J.J. Gooding)

^{*}Mengli Liu and Yuanhong Xu contribute equally to this work.

detection of ferric ions (Fe^{3+}) in tap water as well as for efficient cell imaging.

2. Experimental

2.1 Reagents

Ethanol (AR), sodium hydroxide (AR), methanol (AR), butanol (AR), acetone (AR), potassium phosphate monobasic (99.5%, AR), potassium phosphate dibasic (99%, AR), sulfuric acid (98%, AR), hydrochloric acid (37%, AR) and carbon dioxide were obtained from Shangdong Laiyang Economic and Technological Development Zone Chemical Plant (Shandong, China). Silver nitrate, mercuric nitrate, 3-[4,5-dimethylthiazol-2-yl]-2,5-diphenyltetrazolium bromide (MTT), dimethyl sulfoxide (DMSO), and quinine sulfate were purchased from Aladdin Reagent Co., Ltd (Shanghai, China). Aluminum chloride, sodium sulfate, chromium acetate, ferric chloride, copper chloride, cobalt chloride, ferrous chloride, magnesium chloride, lead acetate, manganese chloride, zinc chloride and nickel nitrate were obtained from Tianjin Reagent Co., Ltd (Tianjin, China). The graphite electrode, a platinum foil electrode and Ag/AgCl (3.0 M NaCl) electrode were purchased from Tianjin Aida Hengsheng Technology Co. Ltd. (Tianjin, China). Ultrapure water was produced using a Flom ultrapure water system (Qingdao, China).

2.2 Apparatus

All electrochemical measurements were performed with a conventional three-electrode cell with a CHI 760D electrochemical workstation (CH Instruments, Shanghai, China). A graphite electrode, a platinum foil electrode and an Ag/AgCl (3.0 M NaCl) electrode were used as the working, counter and reference electrodes, respectively. All potentials were carried out in a one-compartment electrochemical cell at room temperature. The UV-Vis spectra of samples were recorded on a UV-Vis-NIR spectrophotometer (Lambda 950, Perkin Elmer Instruments). Fourier transform infrared (FTIR) spectra were carried out on a Nicolet Nexus 5700 (Thermo Electron Corporation, USA) using KBr pellets. The fluorescence was measured on a Cary Eclipse Fluorescence spectrophotometer (Varian Co., Australia). The excitation/emission slits were set at 5.0×5.0 nm. X-ray photoelectron spectroscopy (XPS) data were obtained on an ESCALab220i-XL electron spectrometer (VG Scientific, West Sussex, U.K.) using 300 W Al $K\alpha$ radiation. Transmission electron microscopy (TEM) images were obtained with a FEI TECNAI G2 transmission electron microscope (Eindhoven, Netherlands) operating voltage of 120 kV.

2.3 Electrochemical Synthesis of CQDs

The preparation of CQDs was carried out with a three-electrode system consisting of a graphite electrode working electrode, a platinum foil counter electrode and an Ag/AgCl reference electrode. Ethanol (35 mL), water (8 mL), and NaOH (0.03 g) mixed to obtain the electrolyte. The potentiostatic voltage of 5 V was applied to the working electrode for 3 h

under the nitrogen ambient (see Scheme 1). The excess NaOH precipitate was removed by centrifugation and homogeneous CQDs dispersion was obtained. The original concentration of the CQDs ($500 \mu\text{g mL}^{-1}$) was calculated based on the weight loss of the graphite electrode and the final dispersion volume. The dispersion was kept at 4 °C or at room temperature, respectively.

2.4 Quantum yield measurements

Quantum yield of the CQDs was determined on the basis of previously established procedure. Typically, quinine sulfate (literature quantum yield 0.54) in 0.1 M H_2SO_4 was chosen as a standard as described.^{23,36} In order to minimize re-absorption effects, the absorbance of the aqueous solution of CQDs and reference sample were kept below 0.10 and 0.05 when excited at 360 nm. Quinine sulfate was dissolved in 0.1 M H_2SO_4 while the CQDs were dissolved in ethanol. The quantum yield of the CQDs was calculated using the equation below.³⁷

$$\Phi_x = \Phi_{ST} \left(\frac{\text{Grad}_x}{\text{Grad}_{ST}} \right) \left(\frac{\eta_x^2}{\eta_{ST}^2} \right)$$

Where the subscripts ST and X refer to quinine sulfate and CQDs respectively, Φ represents the fluorescence quantum yield. Grad represents the gradient from the plot of integrated fluorescence intensity vs. absorbance, and η the refractive index of the solvent.

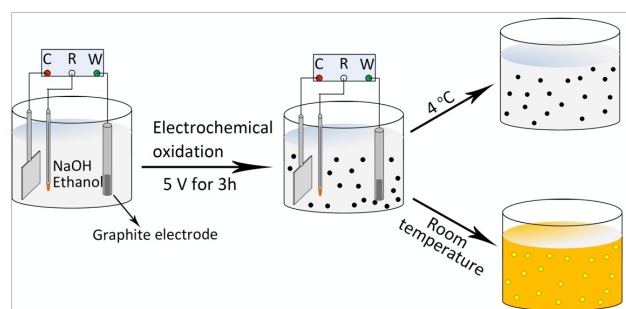
2.5 Detection of Fe^{3+} in tap water

The tap water sample was acidified by diluted with hydrochloric acid prior to analysis. Fe^{3+} at different concentrations (0, 10, 20, 30 and 40 μM) was spiked into the tap water containing 20 $\mu\text{g mL}^{-1}$ bright yellow CQDs, respectively. The PL intensity of the spiked sample was then recorded accordingly. The decrease in PL intensity ($\Delta I = I_0 - I_i$) was plotted against the spiked Fe^{3+} concentration to obtain a calibration curve. The concentration of Fe^{3+} in tap water was calculated based on the absolute value of x-intercept from the calibration curve. The reproducibility of the analysis method was determined by measuring the relative standard deviations of replicate measurements ($n = 3$).

2.6 The intracellular uptake of CQDs, bio-imaging and MTT assays

Bamboo fibre cells (10^6 cells per sample) were plated onto 35 mm glass chamber slides. The bright yellow CQDs dispersion was firstly distilled to remove the ethanol and diluted in deionized water. Then the pH of the final CQDs dispersion was adjusted to 7.4. CQDs dispersion at concentration of 50 $\mu\text{g mL}^{-1}$ in DMEM were then freshly prepared and placed over the cells for 1 h at 37 °C. Subsequently the cells were washed thoroughly three times with PBS to remove extracellular CQDs. Finally, the cellular images were taken by a Leica TCS SP2 confocal laser scanning microscope (CLSM) (Leica Microsystems Heidelberg GmbH, Germany) with excitation wavelength at 365 nm.

MTT assays were used to evaluate the CQDs doses on the viability of the bamboo fibre cells. The cells were treated with



Scheme 1 Schematic illustration for CQDs generation via electrochemical oxidation of graphite electrode in alkaline alcohols and colour change of the dispersion upon storage at room temperature.

various concentrations of CQDs (0, 20, 50, 100, 150, 200, 250 $\mu\text{g mL}^{-1}$) in fresh DMEM for 24 h. Treated cells were added with DMEM containing MTT (10 mL, 5 mg mL^{-1} in PBS solution) and further incubated at 5% CO_2 , 37 $^\circ\text{C}$ for 4 h. Then, the MTT containing medium was added to each well with 100 μL DMSO to solubilize the formazan crystals precipitate. Viability of untreated control cells was arbitrarily defined as 100%. Finally, the absorption at 365 nm of each well was measured by an EL808 ultramicroplate reader (Bio-TEK Instrument, Inc., Winooski, VT, USA).

3. Results and discussion

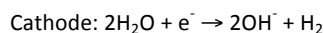
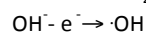
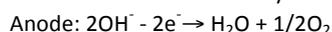
3.1 CQDs generation via the electrochemical oxidation of the GE

As shown in scheme 1, the CQDs were generated via a three-electrode system, where graphite electrode was used as working electrode, a platinum foil as counter and an Ag/AgCl electrode as reference, respectively. Alkaline alcohol (e.g. NaOH/EtOH) was used as electrolyte. When a constant potential of 5 V was applied to the working electrode for 3 h under the nitrogen ambient, the colourless CQDs dispersion was obtained. During the process of the electrochemical oxidation for CQDs generation, the electrolyte remained colourless and the surface of the graphite electrode did not expand substantially. This phenomenon was in contrast to previous reports, where brown CQDs dispersion and an expanded electrode were observed when the graphite rod or other carbon materials were used as working electrode.³⁸ A detailed comparison of methods for producing CQDs electrochemically is shown in Table S1. It can be seen that the EC method using alkaline alcohol as electrolyte is relatively green, low-cost and reproducible for CQDs generation. However, when the colourless dispersion of CQDs was stored at room temperature, the colour of the dispersion slowly turned bright yellow. Nevertheless, the dispersion was still colourless if stored at 4 $^\circ\text{C}$. The influence of different applied potentials (3V, 5V and 7V, respectively) on the preparation of CQDs was investigated. It was found that higher applied potential could result in larger CQDs. As can be seen in Fig. S1, the average sizes of the CQDs obtained at 3 V and 7 V were 2.9 ± 0.3 nm and 5.2 ± 0.6 nm, respectively, indicating that the applied potential played a key role in controlling the size of the C-dots. When the applied potential

was controlled at 3 V, longer synthesis time of 12 h was needed to generate CQDs because of the lower current. When the potential of 7 V was applied, the current was much higher, causing a faster volatilization of ethanol. The quantum yields of the bright yellow CQDs generated at 3 V, 5 V and 7 V were 9.5%, 11.2% and 4.6%, respectively. Therefore, 5 V was found to be the most suitable potential for the preparation of CQDs.

To further confirm whether the CQDs were generated from graphite electrode or from other carbon elements in the electrolyte, several control experiments were performed. It was found that CQDs were also obtained in methanol/NaOH, butanol/NaOH, but not in Na_2SO_4 /ethanol, acetone/NaOH, PBS (PH=7.0)/ethanol or hydrochloric acid/ethanol. These results suggested that both the alcohols and the OH^- groups played important roles in the process of CQDs formation.^{5, 34} When platinum foils or two gold rods were used as working electrodes, no CQDs was obtained under the same electrochemical conditions, although there is a report of the formation of CQDs in low-molecular-weight alcohol electrolytes using Pt as working electrode.³⁴ Taken together, the above results indicated that the carbon source of the as-prepared CQDs came from the graphite electrode.

During the electrochemical reactions, gases were produced on both the anode and cathode due to water splitting, which usually takes place at a potential reaching 1.23 V in moderately concentrated salt solutions. Nevertheless, active intermediates, such as hydroxyl radicals ($\cdot\text{OH}$) can also be generated on the graphite interfaces at the high anodic overpotential (e.g., 5 V). The electrochemical reactions may occur as follows:^{39,40}



The generated hydroxyl radicals corrode the GE at the edges. These radicals produced in alkaline electrolyte without alcohols are nonselective and highly active, causing the fast exfoliation of the larger-size graphite sheets from graphite. Upon addition of alcohols, the activity of the radicals can be moderately controlled, leading to the smooth generation of CQDs.⁴¹⁻⁴³ As a result, the CQDs with hexagonal lattice structure could be electrochemically exfoliated from GE.

3.2 Characterizations of the as-prepared CQDs

To confirm the CQDs formation and explore the reasons for the colour change upon different storage conditions, a variety of methods to characterize the CQDs were performed. Fig. 1 showed the typical transmission electron microscopy (TEM) images and size distributions of colourless (Fig. 1A and 1C) and bright yellow (Fig. 1D and 1F) CQDs, respectively. The TEM images confirmed the formation of CQDs and revealed that the as-synthesized colourless CQDs were monodispersed (Fig. 1A) with an average diameter of (4.0 ± 0.2) nm ($n=200$) (Fig. 1C). Compared with the colourless ones, the bright yellow CQDs gave two size distributions. One was from individual dispersed CQDs and the other caused by some aggregation of CQDs (shown in Fig. 1D) with average size of (8 ± 0.3) nm ($n=200$) (Fig. 1F). The high-resolution TEM (HRTEM) images are shown

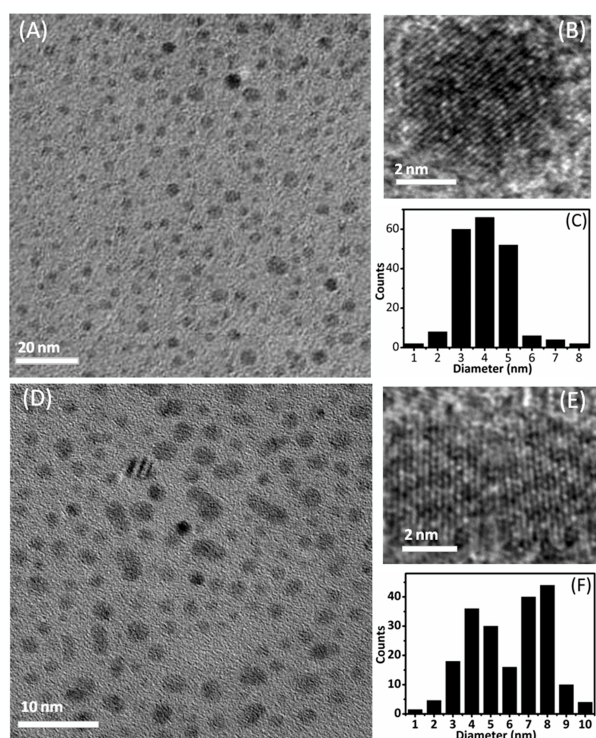


Fig. 1 (A, D) TEM and (B, E) HRTEM images as well as (C, F) size distribution of the colourless and bright yellow CQDs, respectively.

in Fig. 1B and Fig. 1E. It can be seen that the as-prepared CQDs were of high crystallinity and the lattice spacing was around 0.31 nm in the crystalline structures of the CQDs, which agrees well with the $\langle 002 \rangle$ spacing of graphitic carbon.^{44, 45}

FTIR and XPS analyses were performed to investigate the surface functional groups of CQDs. As shown in Fig. 2A, the absorption peaks at $\sim 3438\text{ cm}^{-1}$, $\sim 1634\text{ cm}^{-1}$ and $\sim 1384\text{ cm}^{-1}$ should be assigned to stretching vibrations (ν) of O-H, C=O and bending vibrations (δ) of C-H, respectively. The absorption

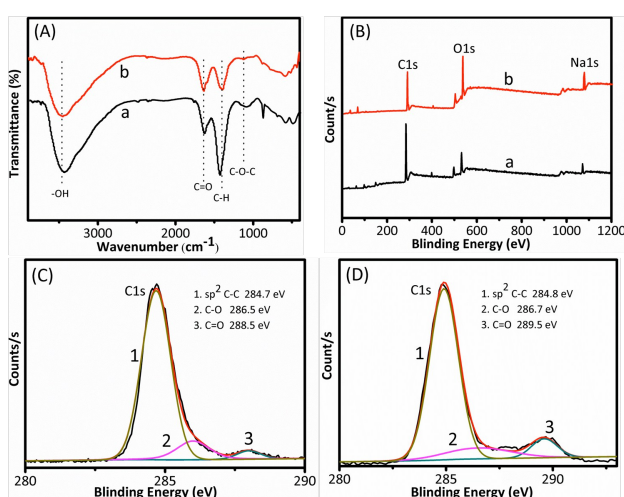


Fig. 2 (A) FT-IR spectra of (a) colourless dispersion and (b) bright yellow dispersion of CQDs. (B) The survey XPS spectra for CQDs in (a) colourless dispersion and (b) bright yellow suspension. Fitting of C1s XPS spectra of (C) colourless dispersion and (D) bright yellow dispersion of CQDs, respectively.

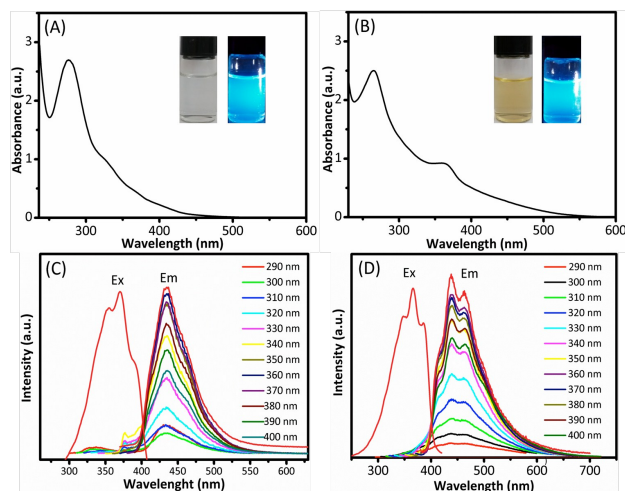


Fig. 3 UV-vis absorption spectra and the corresponding photographs of the colourless CQDs dispersion (A) and bright yellow one (B) under room light (inset, left) and upon irradiation with 365 nm UV light (inset, right), respectively. Emission (Em) spectra at progressively increasing excitation wavelengths from 290 nm to 400 nm and excitation (Ex) spectrum of the colourless CQDs dispersion (C) and bright yellow one (D), respectively.

peak at 1150 cm^{-1} should be attributed to stretching vibrations (ν) of C-O-C. The relative intensity of $\nu_{\text{C=O}}$ and $\delta_{\text{C-H}}$ in the bright yellow dispersion were higher compared with that of the colourless suspension, suggesting that the surface oxidation degree of the bright yellow dispersion was higher than that of colourless one. Moreover, XPS was used to monitor the surface composition of the CQDs. There were three significant peaks corresponding to elemental species C, O, and Na in the survey spectra (Fig. 2B). Fig. 2C and Fig. 2D are the XPS spectra of the colourless and bright yellow CQDs, respectively. The C1s spectrum can be deconvoluted into three peaks, among which the peaks centered at 284.7 or 284.8 eV should be attributed to graphitic sp^2 carbon atoms, and those centered at 286.5 or 286.7 eV and 288.5 or 289.5 eV can be attributed to C-O and C=O, respectively.^{2, 16, 23} As shown in Fig. 3C and Fig. 3D, the intensity ratio between O and C content on the surface of the bright yellow CQDs was higher than that of the colourless one, indicating the higher oxygen content on the CQDs in the bright yellow suspensions than in the colourless one. The XPS analysis results are consistent with the FTIR ones. These results indicate that the CQDs were more easily oxidized at the room temperature, producing oxygen-containing groups (e.g. -COOH) on CQDs. At lower temperature (e.g. $4\text{ }^\circ\text{C}$) the colour of the dispersion did not change over the same time owing to less oxidation of CQDs. Thus the temperature was a determining factor for the oxidation of CQDs. Meanwhile, the carboxyl groups formed by the oxidation invokes more $n \rightarrow \pi^*$ transition and makes the wavelength of the maximum absorption peak shift to the range of visible light. This is one of the reasons why the colour of the CQDs dispersion changed from colourless to yellow upon oxidation in storage at room temperature.

Fig. 3 depicts the UV-Vis and fluorescence spectra of the resultant CQDs in aqueous solutions. Both the colourless and bright yellow CQDs dispersion revealed good dispersibility, and displayed bright blue luminescence under 365 nm UV

irradiation, which evidenced that the CQDs possessed good optical properties. Furthermore, both the CQDs exhibited typical UV/Vis absorption at 280 nm which could be ascribed to the $\pi \rightarrow \pi^*$ transition of the aromatic sp^2 domain within the CQDs.^{16, 20} However, there was another relatively strong absorption at 380 nm for the bright yellow CQDs suspension, which should be resulted from the $n \rightarrow \pi^*$ transition of C=O band,⁴⁶ indicating the increased degree of oxidation of the CQDs from the bright yellow suspension.

The typical PL emission spectra of the CQDs under different excitation wavelengths are shown in Fig. 3C and 3D. The maximum fluorescence emissions appeared at 436 and 438 nm for the colourless and bright yellow CQDs suspensions, respectively, when excited at 365 nm. In addition, the intensities of both the two CQDs suspensions exhibited excitation-dependent PL behaviors, which first increased and then decreased with increasing excitation wavelength from 290 to 400 nm. Interestingly, the maximum emission wavelength of these two kinds of CQDs suspensions remained constant with the excitation wavelength changing, showing the λ_{ex} -independent emission behavior, which should be attributed to the lower degree of oxidation on the graphite electrode in the mild reaction ambient herein.^{2, 5, 33} This is consistent with the previous results that the surface states rising from the surface oxidation prominently impacted the PL properties.³³ Surface oxidation was found to be able to generate surface defects of CQDs,^{47, 48} which would result in more complex surface states of the CQDs to trap more excitons under excitations. Consequently, the radiative recombination of trapped excitons would generate the fluorescence emission with corresponding energy, which led to the red-shifted i.e. λ_{ex} -dependent emission. Meanwhile, the graphite electrode with a lower degree of surface oxidation is expected to exhibit fluorescence emissions with fewer energy bands at different excitations, thus the as-prepared CQDs herein behaved the λ_{ex} -independency behavior.^{1, 4, 33} Compared with the colourless CQDs (Fig. 3C), more peaks were observed in the emission spectrum for the bright yellow CQDs (Fig. 3D), which should be due to the change of particle size distributions upon storage at room temperature (Fig. 1C and 1F).⁴⁹

3.3 Applications

In addition to the distinct optical properties, the obtained CQDs also exhibited good stability. Even after being kept for three month at room temperature, they still showed a transparent appearance and strong PL intensity. Therefore, the CQDs possessed good potentials as nanoparticles in bio-imaging, optical sensing and biological labeling. Subsequently, we demonstrated the application of the CQDs in metal ion detection and cell imaging.

3.3.1 Specific ferric ion (Fe^{3+}) detection

The impact of different metal ions (all at 120 μM) including Fe^{2+} , Fe^{3+} , Hg^{2+} , Mg^{2+} , Mn^{2+} , Co^{2+} , Ni^{2+} , Ag^+ , Al^{3+} , Cd^{2+} , Cu^{2+} , Pb^{2+} , Zn^{2+} on the PL intensity of the CQDs was studied. Before

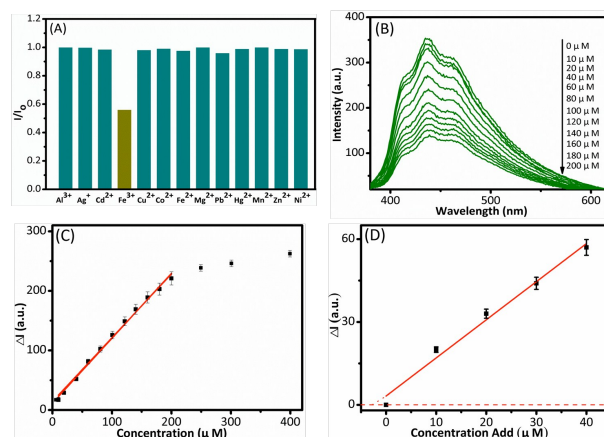


Fig. 4 (A) Remained percentage of the PL intensity of bright yellow CQDs after addition of different metal ions (all at 120 μM) in acidic conditions (pH = 6.0). (B) PL intensity of bright yellow CQDs in the presence of Fe^{3+} ions at different concentrations from 0 to 200 μM . The arrow indicates the change of concentration. (C) Plot of quenched PL intensity ($\Delta I = I_0 - I$) of CQDs against the Fe^{3+} concentrations. (D) Detection of Fe^{3+} ion in tap water using a standard addition method. Excitation at 370 nm was applied. Error bars indicate standard deviations of the means ($n=3$).

performing the experiment, the CQDs suspensions were adjusted to acidic conditions (pH = 6.0), in which the metal ions can exist in their free forms. The fluorescence intensities of CQDs were significantly decreased in the presence of Fe^{3+} , while the other ions displayed weak or even negligible effects on their fluorescence intensities (Fig. 4A). These observations reflected that the fluorescence of CQDs have specific response to Fe^{3+} , and therefore could be used for the assay of Fe^{3+} .

The fluorescence intensities of CQDs upon the addition of different concentrations of Fe^{3+} ranging from 0 to 400 μM are shown in Fig. 4B. Fig. 4C plots the quenched PL intensity ($\Delta I = I_0 - I$) of CQDs against the Fe^{3+} concentrations (C). A linear dependence of ΔI on the concentration of Fe^{3+} from 10 to 200 μM was derived, with a linear regression equation of $\Delta I = 1.09C + 11.50$ and correlation coefficient of 0.9944. The limit of detection (LOD) for Fe^{3+} was figured out to be 1.8 μM ($S/N=3$), which is comparable to the sensitivity of some previous reports^{50,51}. Moreover, the method has the advantages of a wide linear range and a simple preparation procedure.⁵²

The applicability of the proposed methods in real sample analysis was evaluated using a standard addition method for detection of Fe^{3+} in tap water (Fig. 4D). The RSD was 0.36% for 3 replicate measurements for the PL intensity of the tap water sample spiked with 5 μM Fe^{3+} , indicating the good reproducibility of the proposed method. Satisfactory recoveries between 96.3% and 107% were obtained. Linear relationship ($\Delta I = 3.2 + 1.38C$, $R = 0.9859$) was achieved and the Fe^{3+} concentration in tap water was measured to be 2.3 ± 0.1 μM ($n=3$), a value which is very close to that obtained by atomic absorption spectrophotometry (AAS) analysis (2.5 ± 0.2 μM ($n=3$)). The AAS procedure is outlined in the Supporting

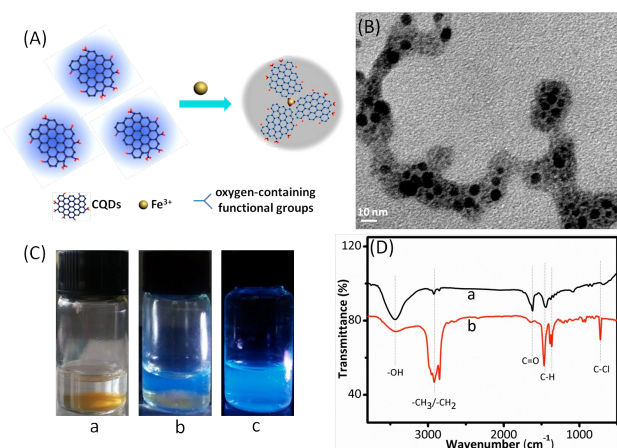


Fig.5 (A) Schematic representation of PL quenching mechanism of CQDs by Fe^{3+} . (B) TEM image of the aggregated CQDs upon addition with Fe^{3+} . (C) the corresponding photographs of the Fe^{3+} -containing CQDs suspension stored for 8 h under room light (a) and under irradiation with 365 nm UV light (b); (c) the photograph of original CQDs under irradiation with 365 nm UV light. (D) FTIR spectra of (a) original CQDs suspension; (b) precipitate formed in Fe^{3+} -containing CQDs suspension stored for 8 h.

Information. The assay shows good selectivity, accuracy and reproducibility for Fe^{3+} detection in real samples.

The PL quenching of CQDs by Fe^{3+} should be ascribed to the specific affinity between Fe^{3+} and the oxygen-containing functional groups such as carboxylic or hydroxyl groups on the surface of the CQDs. The interaction between the CQDs and Fe^{3+} resulted in CQDs aggregation, which appears to have caused the quenching of the CQD's PL (Fig. 5A).^{53, 54} When Fe^{3+} was added to the CQDs suspension, the aggregation of CQDs was observed as evidenced by TEM image (Fig. 5B). The average diameter of the aggregated CQDs was 14 ± 0.8 nm, which was three times larger than that of the original precursor. A yellow precipitate was also observed upon further storage of the Fe^{3+} -containing CQDs suspension for 8 h (Fig. 5C-a). Under irradiation with 365 nm UV light, the blue light of the supernatant (Fig. 5C-b) faded noticeably compared with that of original CQDs suspension (Fig. 5C-c). FTIR spectroscopy was also performed in an attempt to identify any changes in the functional groups on the CQDs treated with and without Fe^{3+} (Fig. 5D). As shown in Fig. 5D-a, the peak at 1634 cm^{-1} , which resulted from C=O stretching, was clearly observed with the original CQDs. However, this peak was hardly apparent with the as-formed precipitate upon the addition of Fe^{3+} (Fig. 5D-b), hence providing evidence for the interaction between the carboxylic acid group and Fe^{3+} . The FTIR spectra were also collected for CQDs upon addition with other ions such as Cu^{2+} , Cd^{2+} and Ni^{2+} . In these cases there was no obvious peak intensity change in FTIR was observed (Fig. S2). This again confirmed the selective affinity interaction between Fe^{3+} and the oxygen-containing groups on the CQDs.

3.3.2 Cell imaging and cytotoxicity measurement

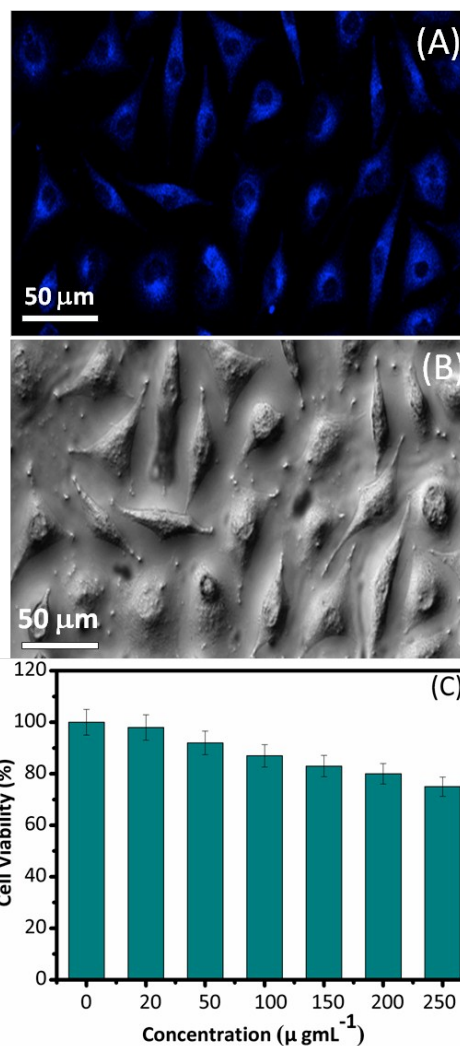


Fig. 6 LSCM images of bamboo fibre cells from mice incubated with CQDs of $50 \mu\text{g mL}^{-1}$ for 2 h at 37°C . (A) Fluorescence images and (B) bright field images; Excitation wavelength was set at 365 nm; (C) Cell viability of bamboo fiber cells ($n=3$, mean \pm S.D.) after being treated with various final concentrations of CQDs (0, 20, 50, 100, 150, 200 and $250 \mu\text{g mL}^{-1}$, respectively). Untreated cells were served as the control, whose viability was set as 100%.

With an attractive set of features including small size, bright luminescence and benign nature, CQDs have a great potential in bio-imaging applications. The application of the obtained CQDs was demonstrated by fluorescence imaging using the bamboo fibre cells of mice as a model. After being incubated with as-prepared CQDs for 1 h at 37°C and 5% CO_2 , the images were collected with a laser scanning confocal microscope. As illustrated in Fig. 6A, the CQDs treated cell became bright blue under 365 nm light excitation. It can be seen that the luminescent spots widely appeared in the membrane and cytoplasmic area of the cells, whereas fluorescence within the nucleus was very weak, suggesting that CQDs could be internalized into the cells outer membrane but were less easily taken up through the nuclear envelope by the nucleus pore complexes. The easy cellular uptake of the

fluorescent CQDs for efficient bio-imaging should be ascribed to the small sizes of CQDs. It has been reported that the nanoparticles with diameter less than 10 nm are favourable for being internalized into the cells.⁵⁵ In this case, genetic disruption of the cells may be avoided, which agrees well with the results of previous investigation on the interaction of living cells with CQDs and other QDs.⁵⁶⁻⁵⁹ Reproducible imaging results were achieved for the cell treated with CQDs. The cytotoxicity of CQDs was further tested by MTT assay (Fig. 6C). The cell viability decreased with the increasing concentrations of the CQDs in the range of 0, 20, 50, 100, 150, 200 and 250 $\mu\text{g mL}^{-1}$, respectively. Survival rates of the cells reached 92% and 80% in the culture medium containing 50 and 200 $\mu\text{g mL}^{-1}$ CQDs. These results demonstrated that the as-prepared CQDs could be used as an excellent fluorescent bio-imaging agent owing to their good biocompatibility and low toxicity.

Conclusions

Herein, CQDs were simply produced from electrochemical oxidation of the graphite electrode in alkaline alcohols. The as-synthesized CQDs were monodisperse with an average diameter of (4.0 ± 0.2) nm and high crystallinity. Meanwhile, an interesting phenomenon was observed, that is, the colour of the CQDs dispersions was colourless during the reaction process and in storage at 4 °C, but it gradually changed to bright yellow when kept at room temperature. Based on adequate characterization and comparison results, it can be concluded that the surface states induced by the surface oxidation mainly accounted for the colour change of the CQDs dispersions as well as non-shifting fluorescence emissions. Size distribution of CQDs explained the number of the peak appearing in the fluorescence spectra. Meanwhile, the as-prepared CQDs were used for specific and sensitive detection of Fe^{3+} with broad linear ranges of 10 - 200 μM as well as a low limit of detection of 1.8 μM ($S/N = 3$). The applicability in tap water and cell imaging were demonstrated, which confirmed that the CQDs can be used as promising candidates for chemical analysis and biological applications.

Acknowledgements

This work was supported by the Natural Science Foundation of China (21305133, 51173087 and 21575071), Qingdao (12-1-4-2-2-jch), and Taishan Scholars Program. JJG acknowledges the generous financial support from the Australian Research Council Australian Research Council Centre of Excellence in Convergent Bio-Nano Science and Technology (CE140100036) and an ARC Australian Laureate Fellowship (FL150100060).

Notes and references

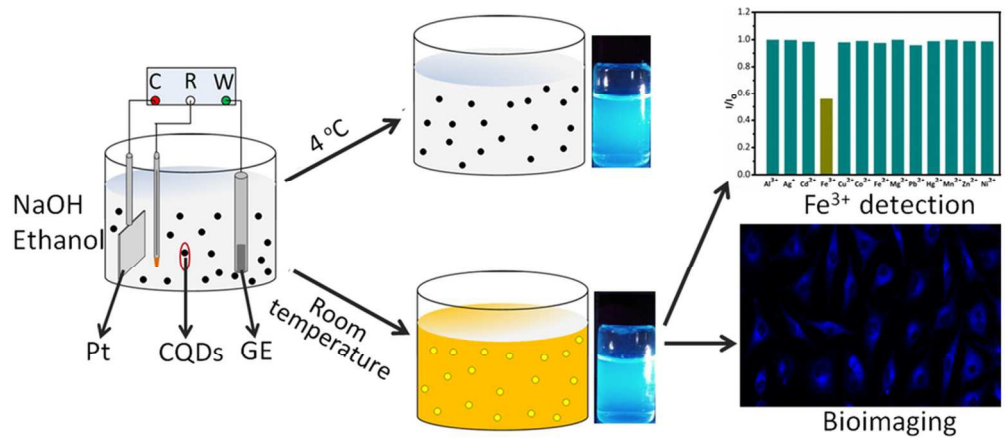
- A. B. Bourlinos, A. Stassinopoulos, D. Anglos, R. Zboril, V. Georgakilas and E. P. Giannelis, *Chem. Mater.*, 2008, **20**, 4539-4541.
- L. Bao, Z.-L. Zhang, Z.-Q. Tian, L. Zhang, C. Liu, Y. Lin, B. Qi and D.-W. Pang, *Adv. Mater.*, 2011, **23**, 5801-5806.
- B. Kong, A. Zhu, C. Ding, X. Zhao, B. Li and Y. Tian, *Adv. Mater.*, 2012, **24**, 5844-5848.
- S. N. Baker and G. A. Baker, *Angew. Chem. Int. Ed.*, 2010, **49**, 6726-6744.
- H. T. Li, X. D. He, Z. H. Kang, H. Huang, Y. Liu, J. L. Liu, S. Y. Lian, C. H. A. Tsang, X. B. Yang and S. T. Lee, *Angew. Chem. Int. Ed.*, 2010, **49**, 4430-4434.
- G. Zhang, C. Li, J. Liu, L. Zhou, R. Liu, X. Han, H. Huang, H. Hu, Y. Liu and Z. Kang, *J. Mater. Chem. A*, 2014, **2**, 8184-8189.
- H. Ming, Z. Ma, Y. Liu, K. Pan, H. Yu, F. Wang and Z. Kang, *Dalton Trans.*, 2012, **41**, 9526-9531.
- Z. Ma, Y.-L. Zhang, L. Wang, H. Ming, H. Li, X. Zhang, F. Wang, Y. Liu, Z. Kang and S.-T. Lee, *ACS Appl. Mater. Inter.*, 2013, **5**, 5080-5084.
- G. Zheng, X. P. A. Gao and C. M. Lieber, *Nano Lett.*, 2010, **10**, 3179-3183.
- G. Zheng, W. L. Daniel and C. A. Mirkin, *J. Am. Chem. Soc.*, 2008, **130**, 9644-9645.
- Y. Li, Y. Hu, Y. Zhao, G. Shi, L. Deng, Y. Hou and L. Qu, *Adv. Mater.*, 2011, **23**, 776-780.
- X. Guo, C.-F. Wang, Z.-Y. Yu, L. Chen and S. Chen, *Chem. Commun.*, 2012, **48**, 2692-2694.
- P. Mirtchev, E. J. Henderson, N. Soheilnia, C. M. Yip and G. A. Ozin, *J. Mater. Chem.*, 2012, **22**, 1265-1269.
- H. Nie, M. Li, Q. Li, S. Liang, Y. Tan, L. Sheng, W. Shi and S. X.-A. Zhang, *Chem. Mater.*, 2014, **26**, 3104-3112.
- Y. Xu, M. Wu, X.-Z. Feng, X.-B. Yin, X.-W. He and Y.-K. Zhang, *Chem.-Eur. J.*, 2013, **19**, 6282-6288.
- Y. Xu, M. Wu, Y. Liu, X.-Z. Feng, X.-B. Yin, X.-W. He and Y.-K. Zhang, *Chem.-Eur. J.*, 2013, **19**, 2276-2283.
- H. Li, J. Liu, M. Yang, W. Kong, H. Huang and Y. Liu, *RSC Adv.*, 2014, **4**, 46437-46443.
- X. Xu, R. Ray, Y. Gu, H. J. Ploehn, L. Gearheart, K. Raker and W. A. Scrivens, *J. Am. Chem. Soc.*, 2004, **126**, 12736-12737.
- L. Y. Zheng, Y. W. Chi, Y. Q. Dong, J. P. Lin and B. B. Wang, *J. Am. Chem. Soc.*, 2009, **131**, 4564-4565.
- Q. L. Zhao, Z. L. Zhang, B. H. Huang, J. Peng, M. Zhang and D. W. Pang, *Chem. Commun.*, 2008, **44**, 5116-5118.
- Y. Q. Dong, C. Q. Chen, J. P. Lin, N. N. Zhou, Y. W. Chi and G. N. Chen, *Carbon*, 2013, **56**, 12-17.
- L. Tian, D. Ghosh, W. Chen, S. Pradhan, X. Chang and S. Chen, *Chem. Mater.*, 2009, **21**, 2803-2809.
- H. Liu, T. Ye and C. Mao, *Angew. Chem. Int. Ed.*, 2007, **46**, 6473-6475.
- H. Zhu, X. L. Wang, Y. L. Li, Z. J. Wang, F. Yang and X. R. Yang, *Chem. Commun.*, 2009, **45**, 5118-5120.
- L. L. Li, J. Ji, R. Fei, C. Z. Wang, Q. Lu, J. R. Zhang, L. P. Jiang and J. J. Zhu, *Adv. Funct. Mater.*, 2012, **22**, 2971-2979.
- M. J. Krysmann, A. Kellarakis, P. Dallas and E. P. Giannelis, *J. Am. Chem. Soc.*, 2012, **134**, 747-750.
- Y.-P. Sun, B. Zhou, Y. Lin, W. Wang, K. A. S. Fernando, P. Pathak, M. J. Mezziani, B. A. Harruff, X. Wang, H. Wang, P. G. Luo, H. Yang, M. E. Kose, B. Chen, L. M. Veca and S.-Y. Xie, *J. Am. Chem. Soc.*, 2006, **128**, 7756-7757.
- A. B. Bourlinos, A. Stassinopoulos, D. Anglos, R. Zboril, M. Karakassides and E. P. Giannelis, *Small*, 2008, **4**, 455-458.
- H. Peng and J. Travas-Sejdic, *Chem. Mater.*, 2009, **21**, 5563-5565.
- J. Zhang, W. Shen, D. Pan, Z. Zhang, Y. Fang and M. Wu, *New J. Chem.*, 2010, **34**, 591-593.
- H. Ming, Z. Ma, Y. Liu, K. Pan, H. Yu, F. Wang and Z. Kang, *Dalton Trans.*, 2012, **41**, 9526-9531.
- J. Zhou, C. Booker, R. Li, X. Zhou, T.-K. Sham, X. Sun and Z. Ding, *J. Am. Chem. Soc.*, 2007, **129**, 744-745.
- Y.-M. Long, C.-H. Zhou, Z.-L. Zhang, Z.-Q. Tian, L. Bao, Y. Lin and D.-W. Pang, *J. Mater. Chem.*, 2012, **22**, 5917-5920.
- J. H. Deng, Q. J. Lu, N. X. Mi, H. T. Li, M. L. Liu, M. C. Xu, L. Tan, Q. J. Xie, Y. Y. Zhang and S. Z. Yao, *Chem.-Eur. J.*, 2014, **20**, 4993-

ARTICLE

Journal Name

- 1
2
3 4999.
4 35. S. Hu, Y. Guo, Y. Dong, J. Yang, J. Liu and S. Cao, *J. Mater. Chem.*,
5 2012, **22**, 12053-12057.
6 36. B. Laleu, M. S. Machado and J. Lacour, *Chem. Commun.*, 2006,
7 42, 2786-2788.
8 37. W. H. Melhuish, *J. Phys. Chem.*, 1961, **65**, 229-235.
9 38. H. Li, L. Chen, H. Wu, H. He and Y. Jin, *Langmuir*, 2014, **30**,
10 15016-15021.
11 39. S. Yang, S. Brüller, Z.-S. Wu, Z. Liu, K. Parvez, K. Parvez, R. Dong,
12 F. Richard, P. Samorì, X. Feng, and K. Müllen, *J. Am. Chem. Soc.*,
13 2015, **137**, 13927-13932.
14 40. M.E. H. Bergmann and J. Rollin, *Catal. Today*, 2007, **124**, 198-
15 203.
16 41. D. Wei, L. Grande, V. Chundi, R. White, C. Bower, P. Andrew and
17 T. Ryhanen, *Chem. Commun.*, 2012, **48**, 1239-1241.
18 42. J. Lu, J.-x. Yang, J. Wang, A. Lim, S. Wang and K. P. Loh, *ACS Nano*,
19 2009, **3**, 2367-2375.
20 43. K. S. Rao, J. Sentilnathan, H. W. Cho, J. J. Wu and M. Yoshimura,
21 *Adv. Funct. Mater.*, 2015, **25**, 298-305.
22 44. J. Liu, M. Shao, X. Chen, W. Yu, X. Liu and Y. Qian, *J. Am. Chem.*
23 *Soc.*, 2003, **125**, 8088-8089.
24 45. Z. Kang, E. Wang, L. Gao, S. Lian, M. Jiang, C. Hu and L. Xu, *J. Am.*
25 *Chem. Soc.*, 2003, **125**, 13652-13653.
26 46. M. Chen, W. Wang and X. Wu, *J. Mater. Chem. B*, 2014, **2**, 3937-
27 3945.
28 47. S. C. Ray, A. Saha, N. R. Jana and R. Sarkar, *J. Phys. Chem. C*,
29 2009, **113**, 18546-18551.
30 48. Q. Wang, H. Zheng, Y. Long, L. Zhang, M. Gao and W. Bai,
31 *Carbon*, 2011, **49**, 3134-3140.
32 49. L. Wang, X. Chen, Y. Lu, C. Liu and W. Yang, *Carbon*, 2015, **94**,
33 472-478.
34 50. A. Ananthanarayanan, X. Wang, P. Routh, B. Sana, S. Lim, D. H.
35 Kim, K. H. Lim, J. Li, and P. Chen, *Adv. Funct. Mater.*, 2014, **24**,
36 3021-3026
37 51. X. Yan, J.-L., Chen, M.-X., Su, F. Yan, B. Li, B. Di, *RSC Advances*,
38 2014, **4**, 22318-22323.
39 52. S. Zhu, Q. Meng, L. Wang, J. Zhang, Y. Song, H. Jin, K. Zhang, H.
40 Sun, H. Wang and B. Yang, *Angew. Chem. Int. Ed.*, 2013, **52**,
41 3953-3957.
42 53. S. Zhang, J. Li, M. Zeng, J. Xu, X. Wang and W. Hu, *Nanoscale*,
43 2014, **6**, 4157-4162.
44 54. Z.-X. Li, L.-F. Zhang, W.-Y. Zhao, X.-Y. Li, Y.-K. Guo, M.-M. Yu and
45 J.-X. Liu, *Inorg. Chem. Commun.*, 2011, **14**, 1656-1658.
46 55. W. Shi, X. Li, and H. Ma, *Angew. Chem.*, 2012, **124**, 6538-6541.
47 56. H. Li, Z. Kang, Y. Liu, and S. -T. Lee, *J. Mater. Chem.*, 2012, **22**,
48 24230-24253.
49 57. I. Yildiz, E. Deniz, B. McCaughan, S. F. Cruickshank, J. F. Callan,
50 and F. M. Raymo, *Langmuir*, 2010, **26**, 11503-11511.
51 58. I. Yildiz, B. McCaughan, S. F. Cruickshank and J. F. Callan, F. M.
52 Raymo, *Langmuir*, 2009, **25**, 7090-7096.
53 59. X. Cheng, E. Hinde, D. M. Owen, S. B. Lowe, P. J. Reece, K. Gaus,
54 and J. J. Gooding, *Adv. Mater.*, 2015, **27**, 6144-6150.
55
56
57
58
59
60

1
2
3
4
5
6
7
8
9
10
11
12
13
14
15
16
17
18
19
20
21
22
23
24
25
26
27
28
29
30
31
32
33
34
35
36
37
38
39
40
41
42
43
44
45
46
47
48
49
50
51
52
53
54
55
56
57
58
59
60



93x40mm (300 x 300 DPI)